MULTIBODY DYNAMICS 2011, ECCOMAS Thematic Conference
J.C. Samin, P. Fisette (eds.)
Brussels, Belgium, 4-7 July 2011

A TWO-NODE SUPERELEMENT DESCRIPTION FOR MODELLING OF FLEXIBLE COMPLEX-SHAPED BEAM-LIKE COMPONENTS

S. E. Boer, R. G. K. M. Aarts, J. P. Meijaard, D. M. Brouwer, J. B. Jonker

Laboratory of Mechanical Automation and Mechatronics, Faculty of Engineering Technology
University of Twente, P.O. Box 217, 7500 AE Enschede, The Netherlands
e-mail: s.e.boer@utwente.nl

Keywords: superelement, model reduction, elastic beam, flexible multibody dynamics

Abstract. *In this paper, a two-node superelement description is proposed for use in multibody models which is capable of modelling flexible complex-shaped beam-like components. Assuming that the deformations with respect to a co-rotational frame remain small, substructuring methods may be used to obtain a dynamical model with reduced mass and stiffness matrices from a linear finite element model. The development of a two-node superelement is established by linking a reduced linear finite element model with a non-linear finite beam element capable of describing large rigid body motion and small elastic deformations. This is achieved by equating their potential and kinetic energies. Two examples are included. A simulation of the spin-up motion of a flexible beam with uniform cross-section and a similar simulation in which the beam is simultaneously excited in the out-of-plane direction. Both examples show good agreement with simulations obtained using non-linear finite beam elements.*

ISBN 978-2-8052-0116-5

1 INTRODUCTION

Flexible links in mechanisms may in many cases be considered slender, i.e. one-dimensional components, which can be correctly modelled by beams. However, the use of beam elements for modelling of flexible complex-shaped beam-like components, requires the determination of equivalent stiffness and mass matrices of sufficient accuracy. In many cases the elastic deformations in a local co-rotational frame may be considered small. This allows the use of reduced order models generated from a standard linear finite element method (FEM), for the modelling of the elastic deformations. These models are also called superelements.

Different model reduction techniques have been proposed in literature for use in multibody models. Lehner and Eberhard [1] propose the use of Krylov-subspace projection methods. Shabana [2] and Cardona [3], [4] among other authors [5], [6], propose the use of dynamic substructuring techniques. All these reduction techniques have in common that they try to find a reduced set of coordinates to accurately describe the dynamical behaviour of the flexible component.

In this paper, a superelement formulation is developed to enhance the modelling capabilities of a non-linear beam element implemented in the SPACAR software [7]. The distinguishing point in the description of this finite element, is the specification of independent deformation modes as generalized deformations that are invariant for arbitrary rigid body motion. The generalized deformations are expressed as analytical functions of the absolute nodal coordinates in a co-rotational context.

We employ the constraint modes of the Craig-Bampton technique [8] to obtain a reduced linear finite element (FE) model described in terms of generalized boundary coordinates. The superelement formulation is established by relating a set of constraint modes with the set of deformation modes of the non-linear beam element. Furthermore, the time derivatives of the generalized boundary coordinates are related to the absolute nodal velocities of the non-linear beam element. The equivalent stiffness and mass matrices are then obtained by equating the potential and kinetic energies of the reduced linear FE model and the non-linear beam element model.

In Section 2 the formulation of the reduced linear FE model and in Section 3 the non-linear beam element model will be described. Then in Section 4 the superelement description is presented. The potential of the proposed methodology is demonstrated on the basis of two spinning beam examples.

2 REDUCED LINEAR FINITE ELEMENT MODEL

Fig.(1) presents a linear FE model of a flexible complex-shaped beam-like component. In order to construct a two-node superelement, boundary nodes p and q are introduced at either side of the component. The local frame, (x', y', z'), in which the FE model is defined, is rotated such that in the initial undeformed state the x'-axis points from boundary node p to q. The nodes on the interface surfaces are rigidly attached to the boundary nodes, such that the boundary nodes define their position and orientation. By means of the constraint modes of the Craig-Bampton method [9] a reduced linear FE model is derived from which a two-node superelement can be established.

Then the nodal displacements $\boldsymbol{u}$ of the linear FE model can be expressed in terms of the boundary node displacements and rotations,

$$\boldsymbol{u} = \boldsymbol{V}\boldsymbol{\eta}, \tag{1}$$

ISBN 978-2-8052-0116-5

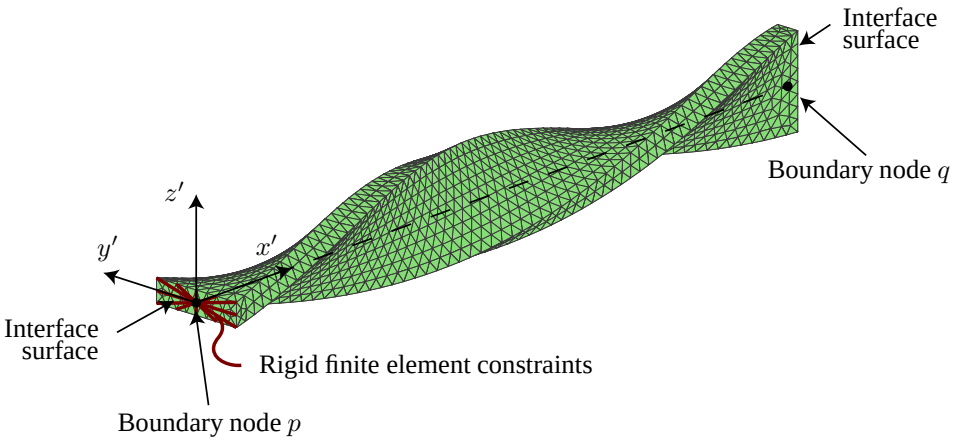

Figure 1: Finite element model of a flexible complex-shaped beam-like component.

where $\boldsymbol{V}$ is the matrix of constraint modes and $\boldsymbol{\eta}$ is the vector with boundary generalized coordinates. A constraint mode is defined as the static deformation of a component, generated by applying a unit displacement on a boundary coordinate while fixing all other boundary coordinates [8]. A total of twelve constraint modes, see Fig. (2), are generated in this way: three rotational and three translational modes at either side. The vector with boundary generalized coordinates is then,

$$\boldsymbol{\eta} = \left[\begin{array}{cccc} \boldsymbol{u}^{p\mathrm{T}} & \boldsymbol{\varphi}^{p\mathrm{T}} & \boldsymbol{u}^{q\mathrm{T}} & \boldsymbol{\varphi}^{q\mathrm{T}} \end{array} \right]^{\mathrm{T}}, \tag{2}$$

where $\boldsymbol{u}^p$, $\boldsymbol{\varphi}^p$, $\boldsymbol{u}^q$ and $\boldsymbol{\varphi}^q$ are the nodal displacement and rotation vectors of boundary nodes p and q respectively.

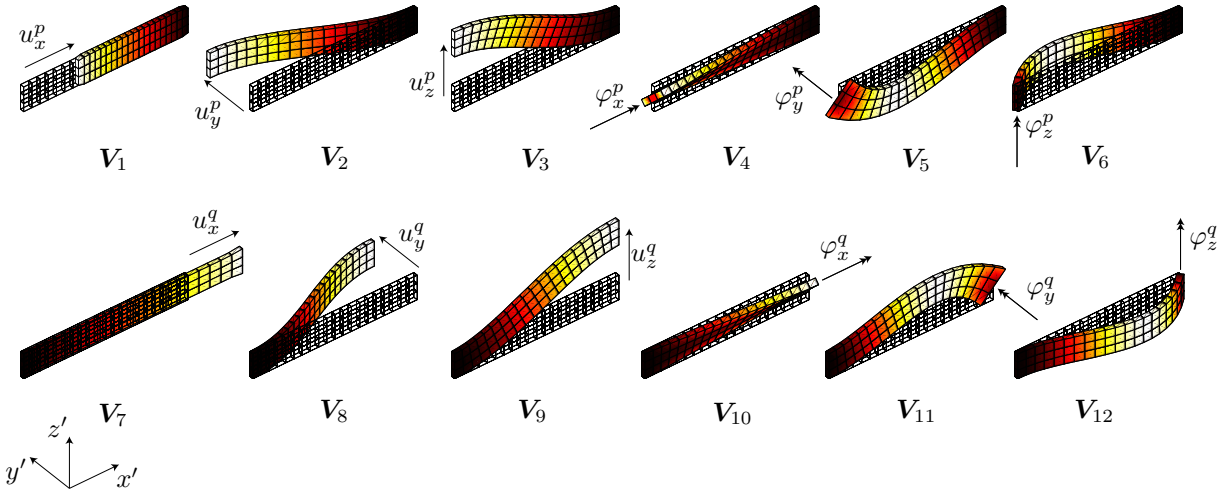

Figure 2: The twelve constraint modes of a simple FE beam model, as they appear column wise in matrix $\boldsymbol{V}$ with corresponding boundary generalized coordinates.

It should be noted that these modes implicitly contain rigid body modes. A 6-D subspace exists in the column space of the constraint mode matrix $\boldsymbol{V}$, that spans the space associated with elastic deformations. A convenient choice for the basis vectors of this subspace are the constraint modes belonging to elongation $\boldsymbol{V}_7$, torsion $\boldsymbol{V}_{10}$, and the four bending modes $\boldsymbol{V}_5$, $\boldsymbol{V}_{11}$, $\boldsymbol{V}_6$ and $\boldsymbol{V}_{12}$. The elastic deformations of the linear FE model can then be expressed as,

$$\boldsymbol{u}_f = \boldsymbol{V}_f \, \boldsymbol{\eta}_f, \tag{3}$$

ISBN 978-2-8052-0116-5

where

$$\boldsymbol{V}_f = \left[\begin{array}{cccccc} \boldsymbol{V}_7 & \boldsymbol{V}_{10} & \boldsymbol{V}_5 & \boldsymbol{V}_{11} & \boldsymbol{V}_6 & \boldsymbol{V}_{12} \end{array} \right], \tag{4}$$

and

$$\boldsymbol{\eta}_f = \left[\begin{array}{cccccc} u_x^q & \varphi_x^q & \varphi_y^p & \varphi_y^q & \varphi_z^p & \varphi_z^q \end{array} \right]^{\mathrm{T}}. \tag{5}$$

Here $\boldsymbol{u}_f$ represents the vector of nodal displacements due to elastic deformation and $\boldsymbol{\eta}_f$ is the vector of elastic boundary generalized coordinates, see Fig.(2).

The potential energy, P_{FEM}, can be expressed as,

$$P_{\mathrm{FEM}} = \frac{1}{2}\boldsymbol{u}_f^{\mathrm{T}}\boldsymbol{K}_{\mathrm{FEM}}\boldsymbol{u}_f \quad = \quad \frac{1}{2}\boldsymbol{\eta}_f^{\mathrm{T}}\bar{\boldsymbol{K}}\boldsymbol{\eta}_f, \tag{6}$$

where

$$\bar{\boldsymbol{K}} = \boldsymbol{V}_f^{\mathrm{T}}\boldsymbol{K}_{\mathrm{FEM}}\boldsymbol{V}_f. \tag{7}$$

Here $\boldsymbol{K}_{\mathrm{FEM}}$ is the stiffness matrix and $\bar{\boldsymbol{K}}$ is the reduced stiffness matrix.

Differentiation of Eq.(1) with respect to time yields,

$$\dot{\boldsymbol{u}} = \boldsymbol{V}\dot{\boldsymbol{\eta}}. \tag{8}$$

The kinetic energy, T_{FEM}, is then defined by

$$T_{\mathrm{FEM}} = \frac{1}{2}\dot{\boldsymbol{u}}^{\mathrm{T}}\boldsymbol{M}_{\mathrm{FEM}}\dot{\boldsymbol{u}} \quad = \quad \frac{1}{2}\dot{\boldsymbol{\eta}}^{\mathrm{T}}\bar{\boldsymbol{M}}\dot{\boldsymbol{\eta}}, \tag{9}$$

where

$$\bar{\boldsymbol{M}} = \boldsymbol{V}^{\mathrm{T}}\boldsymbol{M}_{\mathrm{FEM}}\boldsymbol{V}. \tag{10}$$

Here $\boldsymbol{M}_{\mathrm{FEM}}$ is the mass matrix and $\bar{\boldsymbol{M}}$ is the reduced mass matrix.

3 NON-LINEAR BEAM ELEMENT MODEL

In this section a non-linear beam element will be presented which will serve as a basis for the development of the two-node superelement.

The configuration of the beam element is defined by position vectors $\boldsymbol{x}^p$ and $\boldsymbol{x}^q$ and the orientation of the orthonormal triads, $\left[\boldsymbol{e}_x^p,\ \boldsymbol{e}_y^p,\ \boldsymbol{e}_z^p\right]$ and $\left[\boldsymbol{e}_x^q,\ \boldsymbol{e}_y^q,\ \boldsymbol{e}_z^q\right]$ rigidly attached to the nodes p and q, see Fig.(3). The orientation of the triads can be computed from the initial orientation, $\boldsymbol{R}^e$, and the rotation matrices $\boldsymbol{R}^p$ and $\boldsymbol{R}^q$ which describe the rotation of nodes p and q with respect to the initial orientation,

$$\begin{aligned} \left[\boldsymbol{e}_x^p,\ \boldsymbol{e}_y^p,\ \boldsymbol{e}_z^p\right] &= \boldsymbol{R}^p\boldsymbol{R}^e\left[\boldsymbol{e}_X,\ \boldsymbol{e}_Y,\ \boldsymbol{e}_Z\right], \\ \left[\boldsymbol{e}_x^q,\ \boldsymbol{e}_y^q,\ \boldsymbol{e}_z^q\right] &= \boldsymbol{R}^q\boldsymbol{R}^e\left[\boldsymbol{e}_X,\ \boldsymbol{e}_Y,\ \boldsymbol{e}_Z\right]. \end{aligned} \tag{11}$$

Here $\boldsymbol{e}_X$, $\boldsymbol{e}_Y$ and $\boldsymbol{e}_Z$ are the unit vectors in the global coordinate system. The rotation matrices $\boldsymbol{R}^p$ and $\boldsymbol{R}^q$ can be parametrized in several ways, such as by modified Euler angles, Euler parameters, Rodrigues parameters or the Cartesian rotation vector [10]. We use Euler parameters for the parametrization of rotations, resulting in the following expression for a rotation matrix $\boldsymbol{R}$,

$$\boldsymbol{R} = \boldsymbol{\Lambda}\bar{\boldsymbol{\Lambda}}^{\mathrm{T}}, \tag{12}$$

ISBN 978-2-8052-0116-5

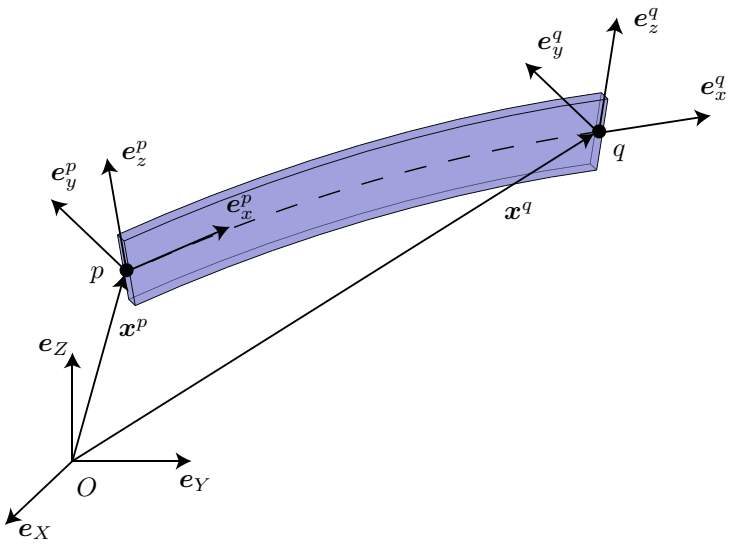

Figure 3: The configuration of the beam element expressed in the global coordinate system (X, Y, Z).

where the matrices $\mathbf{\Lambda}$ and $\bar{\mathbf{\Lambda}}$ are defined by

$$\mathbf{\Lambda} = \begin{bmatrix} -\lambda_1 & \lambda_0 & -\lambda_3 & \lambda_2 \\ -\lambda_2 & \lambda_3 & \lambda_0 & -\lambda_1 \\ -\lambda_3 & -\lambda_2 & \lambda_1 & \lambda_0 \end{bmatrix} \quad \text{and} \quad \bar{\mathbf{\Lambda}} = \begin{bmatrix} -\lambda_1 & \lambda_0 & \lambda_3 & -\lambda_2 \\ -\lambda_2 & -\lambda_3 & \lambda_0 & \lambda_1 \\ -\lambda_3 & \lambda_2 & -\lambda_1 & \lambda_0 \end{bmatrix}, \tag{13}$$

with λ_0, λ_1, λ_2 and λ_3 being the four Euler parameters of the vector $\boldsymbol{\lambda}$. Using Eq. (12) and (13), the rotation matrices $\boldsymbol{R}^p$ and $\boldsymbol{R}^q$ can be written as

$$\boldsymbol{R}^p = \mathbf{\Lambda}^p \bar{\mathbf{\Lambda}}^{p\mathrm{T}}, \tag{14a}$$

$$\boldsymbol{R}^q = \mathbf{\Lambda}^q \bar{\mathbf{\Lambda}}^{q\mathrm{T}}, \tag{14b}$$

where $\mathbf{\Lambda}^p$, $\mathbf{\Lambda}'^p$ and $\mathbf{\Lambda}^q$, $\mathbf{\Lambda}'^q$ are defined by Euler parameter vectors $\boldsymbol{\lambda}^p$ and $\boldsymbol{\lambda}^q$ respectively. Hence, the vector of nodal coordinates, $\boldsymbol{x}$, which defines the positions and rotations of nodes p and q, can then be written as

$$\boldsymbol{x} = \begin{bmatrix} \boldsymbol{x}^{p\mathrm{T}} & \boldsymbol{\lambda}^{p\mathrm{T}} & \boldsymbol{x}^{q\mathrm{T}} & \boldsymbol{\lambda}^{q\mathrm{T}} \end{bmatrix}^{\mathrm{T}}. \tag{15}$$

As the beam element has six degrees of freedom as a rigid body, six independent deformations, characterized by deformation mode coordinates $\boldsymbol{\varepsilon}$, can be expressed as analytical functions of the nodal coordinates [11],

$$\boldsymbol{\varepsilon} = \boldsymbol{\mathcal{D}}(\boldsymbol{x}), \tag{16}$$

ISBN 978-2-8052-0116-5

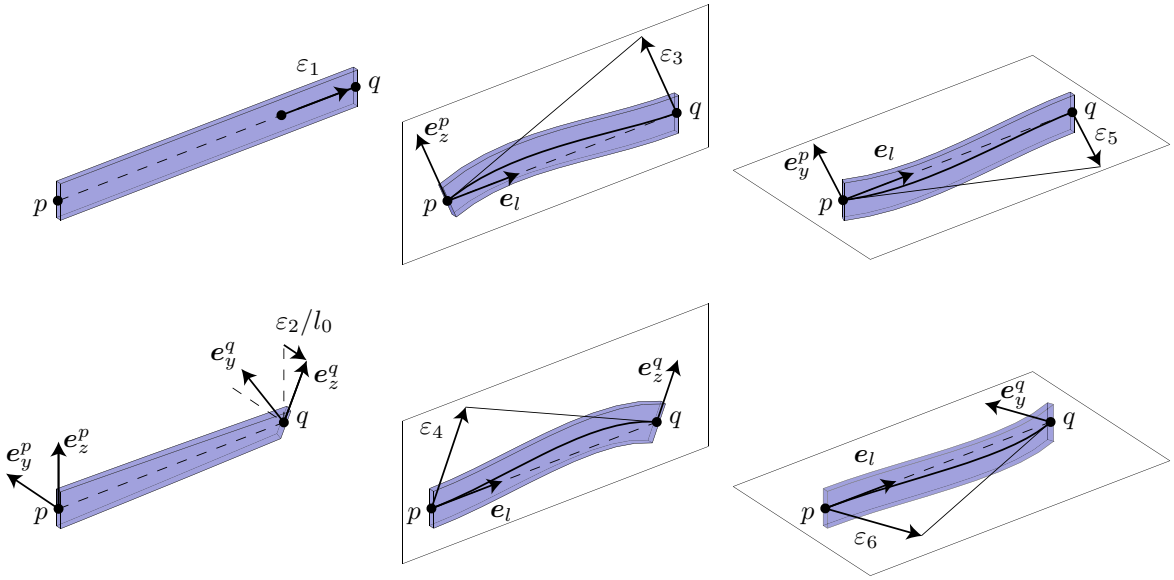

Figure 4: Graphical representation of the generalized deformations ε_1 through ε_6.

where

$$\begin{aligned}
\varepsilon_1 &= l - l_0, \\
\varepsilon_2 &= l_0 \left(\boldsymbol{e}_z^p \cdot \boldsymbol{e}_y^q - \boldsymbol{e}_y^p \cdot \boldsymbol{e}_z^q \right) /2, \\
\varepsilon_3 &= -l_0 \boldsymbol{e}_l \cdot \boldsymbol{e}_z^p, \\
\varepsilon_4 &= l_0 \boldsymbol{e}_l \cdot \boldsymbol{e}_z^q, \\
\varepsilon_5 &= l_0 \boldsymbol{e}_l \cdot \boldsymbol{e}_y^p, \\
\varepsilon_6 &= -l_0 \boldsymbol{e}_l \cdot \boldsymbol{e}_y^q,
\end{aligned} \tag{17}$$

$$\text{with} \quad l = \|\boldsymbol{x}^q - \boldsymbol{x}^p\| \quad \text{and} \quad \boldsymbol{e}_l = \left(\boldsymbol{x}^q - \boldsymbol{x}^p\right)/l.$$

Here l_0 is the original length of the beam element. The deformation mode coordinates can be represent a set of generalized deformations, where the first generalized deformation, ε_1, describes the elongation of the element, the second one, ε_2, describes the torsion and the remaining four are the bending deformations. The generalized deformations ε_{1-6} are visualized in Fig. (4). All generalized deformations are invariant under arbitrary rigid body motion.

The potential energy, P_{Beam}, of the non-linear beam element can be expressed in terms of the generalized deformations

$$P_{\text{Beam}} = \frac{1}{2} \boldsymbol{\varepsilon}^{\mathrm{T}} \boldsymbol{S} \boldsymbol{\varepsilon}, \tag{18}$$

where $\boldsymbol{S}$ is the element stiffness matrix.

The kinetic energy, T_{Beam}, of the non-linear beam element can be expressed as

$$T_{\text{Beam}} = \frac{1}{2} \dot{\boldsymbol{x}}^{\mathrm{T}} \boldsymbol{M} \dot{\boldsymbol{x}}, \tag{19}$$

where $\boldsymbol{M}$ is the element mass matrix and $\dot{\boldsymbol{x}}$ is defined by

$$\dot{\boldsymbol{x}} = \begin{bmatrix} \dot{\boldsymbol{x}}^{p\mathrm{T}} & \dot{\boldsymbol{\lambda}}^{p\mathrm{T}} & \dot{\boldsymbol{x}}^{q\mathrm{T}} & \dot{\boldsymbol{\lambda}}^{q\mathrm{T}} \end{bmatrix}^{\mathrm{T}}. \tag{20}$$

ISBN 978-2-8052-0116-5

4 SUPERELEMENT DESCRIPTION

By linking the reduced linear FE model to the non-linear beam element model, a two-node superelement is created that is capable of representing large rigid body motion and small local flexibilities of complex-shaped beam-like components. This is achieved by equating the potential and kinetic energies of the non-linear beam element model and the reduced linear FE model.

4.1 Kinematics

In order to equate the potential energies, the elastic coordinates of the reduced linear FE model, $\boldsymbol{\eta}_f$ in Eq.(3), should be related to the deformation mode coordinates, $\boldsymbol{\varepsilon}$ in Eq.(17) of the non-linear beam element model. From Fig.(2) and Fig. (4) it can be observed that the vectors $\boldsymbol{\eta}_f$ and $\boldsymbol{\varepsilon}$ can be related by the transformation

$$\boldsymbol{\eta}_f = \boldsymbol{A}\boldsymbol{\varepsilon} \tag{21}$$

where

$$\boldsymbol{A} = \mathrm{diag}\left(\left[\begin{array}{ccccc} 1, & \frac{1}{l_0}, & -\frac{1}{l_0}, & \frac{1}{l_0}, & -\frac{1}{l_0}, \quad \frac{1}{l_0} \end{array}\right]\right), \tag{22}$$

In order to equate the kinetic energies, the velocity vector $\dot{\boldsymbol{\eta}}$ in Eq.(8) should be related to the absolute nodal velocities, $\dot{\boldsymbol{x}}$ in Eq.(20). This is achieved by expressing the components of the absolute nodal velocity vector $\dot{\boldsymbol{x}}$ in the local frame, (x', y', z'), in which the reduced linear FE model is defined. The exact orientation of the local frame is not known, however assuming that only small local deformations occur, a good approximation of this frame can be derived by averaging the orientation of orthonormal triads $\left[\boldsymbol{e}_x^p,\ \boldsymbol{e}_y^p,\ \boldsymbol{e}_z^p\right]$ and $\left[\boldsymbol{e}_x^q,\ \boldsymbol{e}_y^q,\ \boldsymbol{e}_z^q\right]$ defined in Eq.(11). The average orientation, $\boldsymbol{R}^r$, with respect to the initial undeformed orientation, $\boldsymbol{R}^e$, can be computed from the average Euler parameter vector $\boldsymbol{\lambda}^r$,

$$\boldsymbol{\lambda}^r = \frac{\boldsymbol{\lambda}^p + \boldsymbol{\lambda}^q}{\|\boldsymbol{\lambda}^p + \boldsymbol{\lambda}^q\|}, \tag{23}$$

where the differences between $\boldsymbol{\lambda}^p$ and $\boldsymbol{\lambda}^q$ are assumed to be small. According to Eq.(12), the averaged orientation, $\boldsymbol{R}^r$, is then

$$\boldsymbol{R}^r = \boldsymbol{\Lambda}^r \bar{\boldsymbol{\Lambda}}^{r\mathrm{T}}. \tag{24}$$

The local translational velocities in node p can be expressed in terms of $\dot{\boldsymbol{x}}^p$ using the average orientation, $\boldsymbol{R}^r$, and the initial undeformed orientation, $\boldsymbol{R}^e$,

$$\dot{\boldsymbol{u}}^p \approx \boldsymbol{R}^{e\mathrm{T}} \boldsymbol{R}^{r\mathrm{T}} \dot{\boldsymbol{x}}^p, \tag{25}$$

where $\dot{\boldsymbol{u}}^p$ are absolute translational velocities, i.e. they include both rigid body and elastic deformation velocities, expressed in the local frame (x', y', z').

Furthermore, the angular velocity vector, $\dot{\boldsymbol{\varphi}}^p$, can be approximated by,

$$\dot{\boldsymbol{\varphi}}^p \approx \boldsymbol{R}^{e\mathrm{T}} \boldsymbol{R}^{r\mathrm{T}} \boldsymbol{\omega}^p, \tag{26}$$

where $\boldsymbol{\omega}^p$ is the absolute angular velocity vector, with components relative to the global coordinate system (X, Y, Z). An alternative approximation is given by,

$$\dot{\boldsymbol{\varphi}}^p \approx \boldsymbol{R}^{e\mathrm{T}} \bar{\boldsymbol{\omega}}^p, \tag{27}$$

ISBN 978-2-8052-0116-5

where $\bar{\boldsymbol{\omega}}^p$ represents the absolute angular velocity vector with components expressed in the local coordinate system attached to node p. This approximation is also investigated by Cardona [4]. The vectors $\boldsymbol{\omega}^p$ and $\bar{\boldsymbol{\omega}}^p$ are related to the time derivatives of the Euler parameters by the linear transformations

$$\boldsymbol{\omega}^p = 2\boldsymbol{\Lambda}^p \dot{\boldsymbol{\lambda}}^p \tag{28}$$

and

$$\bar{\boldsymbol{\omega}}^p = 2\bar{\boldsymbol{\Lambda}}^p \dot{\boldsymbol{\lambda}}^p. \tag{29}$$

Equivalent relations can be derived for node q. In matrix form Eq.(28), Eq.(26) and Eq.(25) may be combined as,

$$\begin{Bmatrix} \dot{\boldsymbol{u}}^p \\ \dot{\boldsymbol{\varphi}}^p \\ \dot{\boldsymbol{u}}^q \\ \dot{\boldsymbol{\varphi}}^q \end{Bmatrix} = \begin{bmatrix} \boldsymbol{R}^{e\mathrm{T}}\boldsymbol{R}^{r\mathrm{T}} & & & \\ & 2\boldsymbol{R}^{e\mathrm{T}}\boldsymbol{R}^{r\mathrm{T}}\boldsymbol{\Lambda}^p & & \\ & & \boldsymbol{R}^{e\mathrm{T}}\boldsymbol{R}^{r\mathrm{T}} & \\ & & & 2\boldsymbol{R}^{e\mathrm{T}}\boldsymbol{R}^{r\mathrm{T}}\boldsymbol{\Lambda}^q \end{bmatrix} \begin{Bmatrix} \dot{\boldsymbol{x}}^p \\ \dot{\boldsymbol{\lambda}}^p \\ \dot{\boldsymbol{x}}^q \\ \dot{\boldsymbol{\lambda}}^q \end{Bmatrix} \tag{30a}$$

or

$$\dot{\boldsymbol{\eta}} = \boldsymbol{B}_1 \dot{\boldsymbol{x}}. \tag{30b}$$

Alternatively, combining Eq.(29, Eq.(27) and Eq.(25) yields,

$$\begin{Bmatrix} \dot{\boldsymbol{u}}^p \\ \dot{\boldsymbol{\varphi}}^p \\ \dot{\boldsymbol{u}}^q \\ \dot{\boldsymbol{\varphi}}^q \end{Bmatrix} = \begin{bmatrix} \boldsymbol{R}^{e\mathrm{T}}\boldsymbol{R}^{r\mathrm{T}} & & & \\ & 2\boldsymbol{R}^{e\mathrm{T}}\bar{\boldsymbol{\Lambda}}^p & & \\ & & \boldsymbol{R}^{e\mathrm{T}}\boldsymbol{R}^{r\mathrm{T}} & \\ & & & 2\boldsymbol{R}^{e\mathrm{T}}\bar{\boldsymbol{\Lambda}}^q \end{bmatrix} \begin{Bmatrix} \dot{\boldsymbol{x}}^p \\ \dot{\boldsymbol{\lambda}}^p \\ \dot{\boldsymbol{x}}^q \\ \dot{\boldsymbol{\lambda}}^q \end{Bmatrix} \tag{31a}$$

or

$$\dot{\boldsymbol{\eta}} = \boldsymbol{B}_2 \dot{\boldsymbol{x}}, \tag{31b}$$

The matrices $\boldsymbol{B}_1$ and $\boldsymbol{B}_2$ from Eq.(30b) and Eq.(31b) respectively, are referred to as nodal velocity transformation matrices from here on.

4.2 Dynamics

The equivalent stiffness and mass matrices are derived by equating the potential and kinetic energies of the reduced linear FE model and the non-linear beam element. Equating the potential energies of Eq.(6) and Eq.(18) yields,

$$P \quad = \quad \frac{1}{2}\boldsymbol{\varepsilon}^{\mathrm{T}}\boldsymbol{A}^{\mathrm{T}}\bar{\boldsymbol{K}}\boldsymbol{A}\boldsymbol{\varepsilon} \quad = \quad \frac{1}{2}\boldsymbol{\varepsilon}^{\mathrm{T}}\boldsymbol{S}\boldsymbol{\varepsilon}, \tag{32}$$

where Eq.(21) is substituted in Eq.(6). From Eq.(32) it can be observed that

$$\boldsymbol{S} = \boldsymbol{A}^{\mathrm{T}}\bar{\boldsymbol{K}}\boldsymbol{A}. \tag{33}$$

Equating the kinetic energies of Eq.(9) and Eq.(19) yields,

$$T \quad = \quad \frac{1}{2}\dot{\boldsymbol{x}}^{\mathrm{T}}\boldsymbol{B}_i^{\mathrm{T}}\bar{\boldsymbol{M}}\boldsymbol{B}_i\dot{\boldsymbol{x}} \quad = \quad \frac{1}{2}\dot{\boldsymbol{x}}^{\mathrm{T}}\boldsymbol{M}\dot{\boldsymbol{x}} \quad \text{with} \quad i = 1, 2 \tag{34}$$

where Eq.(30b) or Eq.(31b) is substituted in Eq.(9) and $\boldsymbol{B}_i$ denotes either $\boldsymbol{B}_1$ or $\boldsymbol{B}_2$ depending on which transformation matrix is substituted. From Eq.(34) it can be observed that

$$\boldsymbol{M} = \boldsymbol{B}_i^{\mathrm{T}}\bar{\boldsymbol{M}}\boldsymbol{B}_i \tag{35}$$

ISBN 978-2-8052-0116-5

The virtual work done by external forces, $\boldsymbol{f}_{\text{ext}}$, should be equal to the virtual work absorbed by inertial forces, $\boldsymbol{f}_{\text{in}}$, and internal generalized stresses, $\boldsymbol{\sigma}$,

$$\delta \boldsymbol{x}^{\mathrm{T}} \boldsymbol{f}_{\text{ext}} = -\delta \boldsymbol{x}^{\mathrm{T}} \boldsymbol{f}_{\text{in}} + \delta \boldsymbol{\varepsilon}^{\mathrm{T}} \boldsymbol{\sigma}, \tag{36}$$

Using Lagrange's equations, the virtual work done by external forces can also be expressed in terms of kinetic and potential energy,

$$\delta \boldsymbol{x}^{\mathrm{T}} \boldsymbol{f}_{\text{ext}} = \delta \boldsymbol{x}^{\mathrm{T}} \left(\frac{d}{dt} \left(\frac{\partial T}{\partial \dot{\boldsymbol{x}}} \right) - \frac{\partial T}{\partial \boldsymbol{x}} + \frac{\partial P}{\partial \boldsymbol{x}} \right)^{\mathrm{T}}. \tag{37}$$

Substituting the potential and kinetic energy expressions of Eq.(32) and Eq.(34) in Eq.(37) and evaluating the derivatives gives

$$\delta \boldsymbol{x}^{\mathrm{T}} \boldsymbol{f}_{\text{ext}} = \delta \boldsymbol{x}^{\mathrm{T}} \left(\boldsymbol{M} \ddot{\boldsymbol{x}} + \left(\left(\dot{\boldsymbol{B}}_i - \boldsymbol{B}_i^* \right)^{\mathrm{T}} \bar{\boldsymbol{M}} \boldsymbol{B}_i + \boldsymbol{B}_i^{\mathrm{T}} \bar{\boldsymbol{M}} \dot{\boldsymbol{B}}_i \right) \dot{\boldsymbol{x}} \right) + \delta \boldsymbol{\varepsilon}^{\mathrm{T}} \boldsymbol{S} \boldsymbol{\varepsilon}, \tag{38}$$

where $\dot{\boldsymbol{B}}$ and $\boldsymbol{B}^*$ are respectively defined by

$$\dot{B}_{ij} = \frac{\partial B_{ij}}{\partial x_k} \dot{x}_k \quad \text{and} \quad B^*_{ij} = \frac{\partial B_{ik}}{\partial x_j} \dot{x}_k. \tag{39}$$

By comparing Eq.(36) with Eq.(38), the inertial forces and generalized stresses are expressed as,

$$\boldsymbol{f}_{\text{in}} = -\left(\boldsymbol{M} \ddot{\boldsymbol{x}} + \boldsymbol{h} \right) \quad \text{with} \quad \boldsymbol{h} = \left(\left(\dot{\boldsymbol{B}}_i - \boldsymbol{B}_i^* \right)^{\mathrm{T}} \bar{\boldsymbol{M}} \boldsymbol{B}_i + \boldsymbol{B}_i^{\mathrm{T}} \bar{\boldsymbol{M}} \dot{\boldsymbol{B}}_i \right) \dot{\boldsymbol{x}}, \tag{40a}$$

$$\boldsymbol{\sigma} = \boldsymbol{S} \boldsymbol{\varepsilon}, \tag{40b}$$

where $\boldsymbol{M}$ and $\boldsymbol{S}$ are the equivalent mass and stiffness matrices and $\boldsymbol{h}$ are the velocity dependent inertial forces.

5 EXAMPLES

5.1 Spinning beam

The performance of the two-node superelement is demonstrated by analyzing the spin-up motion of a planar flexible beam with uniform cross-section from Ref. [12], see Fig.(5(a)). The beam has a length $L = 8.0\ \mathrm{m}$ with a rectangular cross-section of $0.03675\ \mathrm{m}$ by $0.001986\ \mathrm{m}$, so the area is $A = 7.299 \cdot 10^{-5}\ \mathrm{m}^2$ and the moment of inertia is $I = 8.218 \cdot 10^{-9}\ \mathrm{m}^4$. It is made of aluminum with density $\rho = 2766\ \mathrm{kg/m}^3$ and Young's modulus $E = 6.895 \cdot 10^{10}\ \mathrm{N/m}^2$. The beam is accelerated from rest to a constant angular velocity. The prescribed spin-up motion is given by,

$$e(t) = \begin{cases} 0, & t < 0, \\ \dfrac{\Omega}{T} \left[\dfrac{1}{2} t^2 + \dfrac{T^2}{4\pi^2} \left(\cos \dfrac{2\pi t}{T} - 1 \right) \right], & 0 \le t \le T, \\ \Omega \left(t - \dfrac{1}{2} T \right), & t > T. \end{cases} \tag{41}$$

The final angular velocity is $\Omega = 4\ \mathrm{rad/s}$ and the spin-up time is $T = 15\ \mathrm{s}$, see Fig.(5(b)).

ISBN 978-2-8052-0116-5

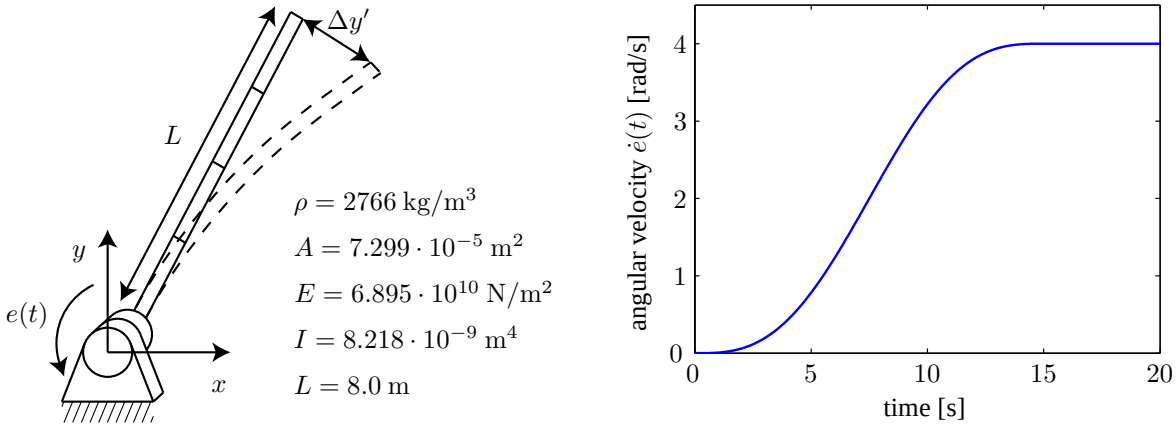

(a) Model parameters (b) Angular velocity profile

Figure 5: Spinning beam model parameters (a) and angular velocity profile (b).

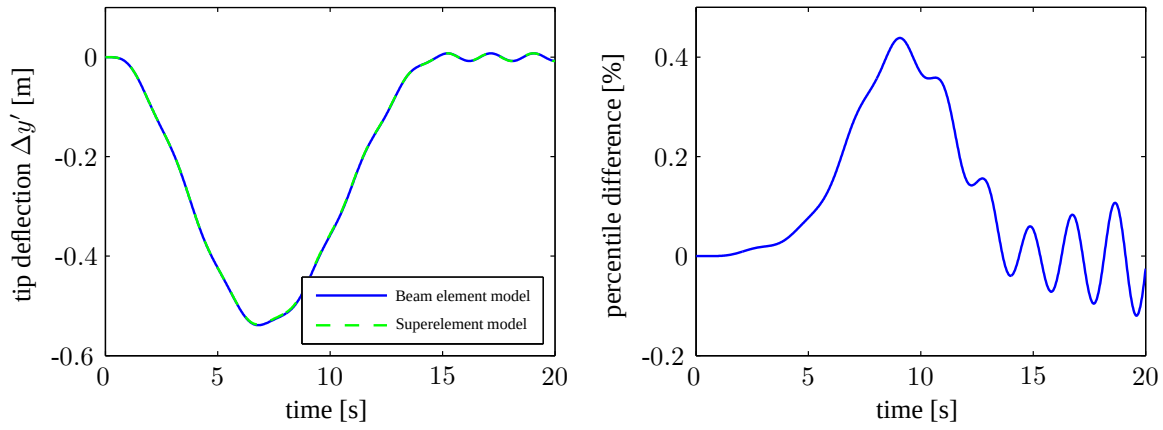

(a) Tip response (b) Tip deflection $\Delta y'$ differences

Figure 6: Tip deflection $\Delta y'$ (a) and percentile difference (b) of the non-linear beam elements and superelements model. Percentile difference is computed with respect to the maximal tip deflection $\Delta y'_{max} = 0.5388\ \mathrm{m}$.

Fig.(6) shows the tip deflection $\Delta y'$ computed by means of the superelement model and the the model with four non-linear beam elements. A single superelement is based on a linear FE model of a beam created using a large number of solid elements. Only a small relative difference between the beam and the superelement model can be observed. During the first 15 seconds of the spin-up motion, the maximal difference is only about 0.4%. Identical results were obtained for the superelement model with velocity transformation matrices $\boldsymbol{B}_1$ and $\boldsymbol{B}_2$ from Eq.(30b) and Eq.(31b) respectively.

Model	number of elements	Max. deflection [m]
SPACAR, non-linear	4	0.5388
SPACAR, superelement	4 superelements	0.5375
Wu and Haug [13]	4 substructures	0.556
idem	6 substructures	0.543

Table 1: Comparison of maximum tip deflections.

In table 1 the values of the maximum tip deflection, obtained by the non-linear beam element

ISBN 978-2-8052-0116-5

and superelement models, are compared with existing results. It can be concluded that they are quantitatively in good agreement.

5.2 Spinning beam with out-of-plane bending

In a second example we consider a spatial beam which is connected by means of a universal joint to a point O fixed in space, see Fig.(7). The universal joint is modelled by two hinges with axes that initially coincide with the global Y- and Z-axes. The relative rotation angles are denoted by e_1 and e_2 respectively, where $e_1(t)$ provides the spin-up motion described by Eq.(41) and $e_2(t)$ represents an additional excitation,

$$e_2(t) = 0.01 \sin(15t)\,. \tag{42}$$

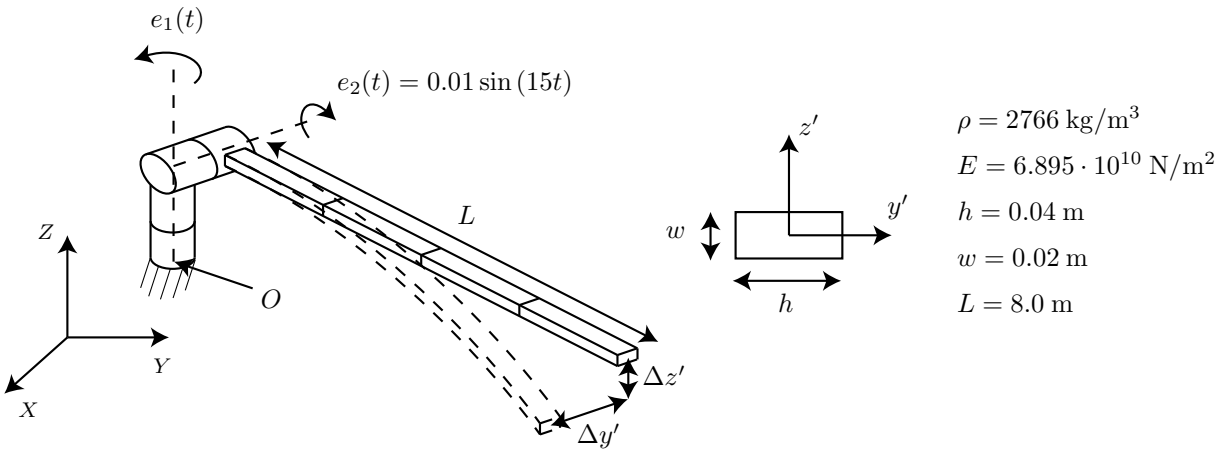

Figure 7: Spinning beam model parameters with out-of-plane excitation.

Fig.(8) and Fig.(9) show the tip deflections $\Delta y'$ and $\Delta z'$ in the horizontal and vertical directions as is depicted in Fig.(7). From the zoomed-in results shown in Fig.(8(b)) and Fig.(9(b)) it can be observed that the superelement models are in good agreement with the non-linear beam elements model. The superelement model with nodal velocity transformation matrix $\boldsymbol{B}_2$ performs slightly better than with transformation matrix $\boldsymbol{B}_1$. This result is also repeatedly observed by Cardona [4].

ISBN 978-2-8052-0116-5

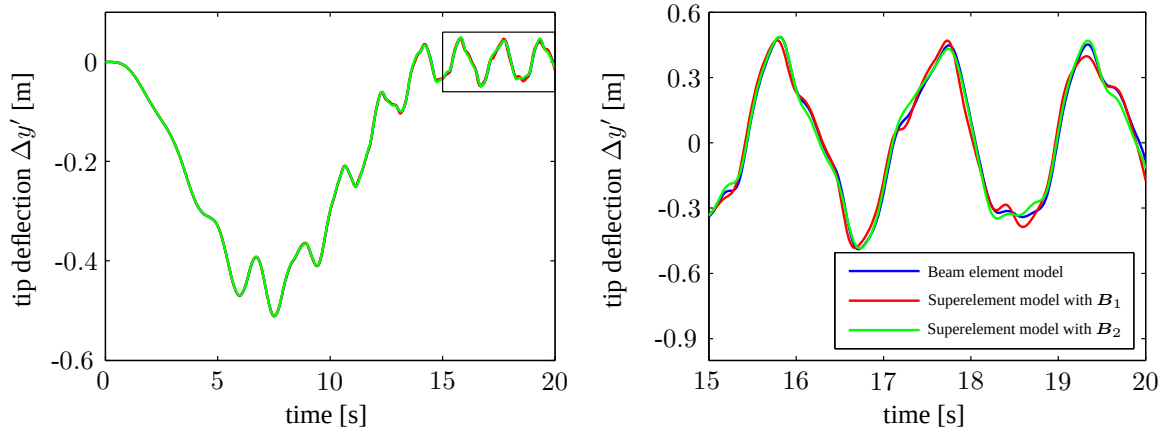

(a) Tip response y-direction (b) Zoom-in of tip deflections $\Delta y'$

Figure 8: Tip deflection $\Delta y'$ (a) and a zoomed-in view of the tip deflections (b) of the non-linear beam elements and the superelement models.

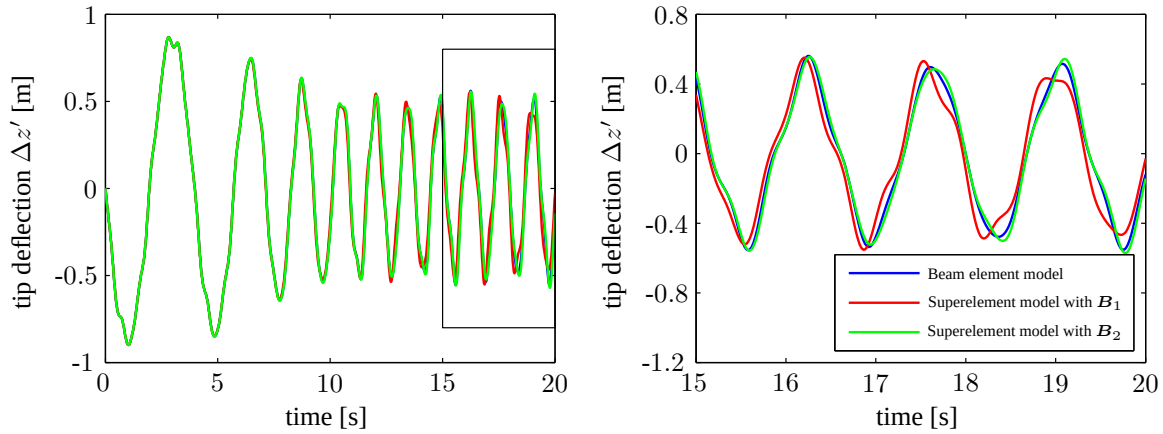

(a) Tip response z-direction (b) Zoom-in of tip deflections $\Delta z'$

Figure 9: Tip deflection $\Delta z'$ (a) and a zoomed-in view of the tip deflections (b) of the non-linear beam elements and the superelement models.

6 CONCLUSIONS

In this paper a two-node superelement is proposed to enhance the modelling capabilities of a non-linear beam element. Two different approaches for the transformation of absolute nodal velocities are considered. In the first approach, absolute translational and angular nodal velocities are expressed in a local approximate frame. In the second approach, the absolute angular nodal velocities are expressed in the local coordinate system attached to the nodes. From the numerical examples it can be observed that the results obtained with both approaches are in good agreement with existing non-linear beam element solutions.

Currently, the reduced linear FE model is described by twelve constraint modes. Only the static deformation of the flexible beam-like component is correctly preserved in this way. In future work the clamped-clamped normal modes, as in the Craig-Bampton method, will be added for more accurate reduced dynamical models.

ISBN 978-2-8052-0116-5

REFERENCES

[1] M. Lehner and P. Eberhard, On the use of moment-matching to build reduced order models in flexible multibody dynamics, *Multibody System Dynamics*, **16**, 191–211, 2006.

[2] A. A. Shabana, Substructure synthesis methods for dynamic analysis of multi-body systems, *Computers and Structures*, **20**, 737–744, 1985.

[3] A. Cardona and M. Géradin, A superelement formulation for mechanism analysis, *Computer Methods in Applied Mechanics and Engineering*, **100**, 1–29, 1992.

[4] A. Cardona, Superelements Modelling in Flexible Multibody Dynamics, *Multibody System Dynamics*, **4**, 245–266, 2000.

[5] O.P. Agrawal and A. A. Shabana, Dynamic analysis of multibody systems using component modes, *Computers and Structures*, **21**, 1303–1312, 1985.

[6] O. A. Bauchau and J. Rodriguez, Formulation of Modal-Based Elements in Nonlinear Flexible Multibody Dynamics, *International Journal for Multiscale Computational Engineering*, **1**, 161–179, 2003.

[7] J. B. Jonker and J. P. Meijaard, *SPACAR – Computer program for dynamic analysis of flexible spatial mechanisms and manipulators*, Multibody Systems Handbook, W. Schiehlen (ed.), 123–143, Springer-Verlag, Berlin, 1990.

[8] R. R. Craig, Jr., Substructure Methods in Vibration, *Journal of Vibration and Acoustics*, **117**, 207-213, 1995.

[9] R. R. Craig, Jr. and M. C. C. Bampton, Coupling of Substructures for Dynamic Analyses, *American Institute of Aeronautics and Astronautics Journal*, **6**, 1313–1319, 1968.

[10] M. Géradin and A. Cardona. *Flexible multibody dynamics: A finite element approach*, John Wiley and Sons Ltd, Chichester 2001.

[11] J.B. Jonker and J.P. Meijaard, Definition of deformation parameters for the beam element and their use in flexible multibody system analysis, ECCOMAS Thematic Conference Multibody Dynamics, Warsaw University of Technology, June 29 – July 2, 2009.

[12] S. S. Kim and E.J. Hang, A recursive formulation for flexible multibody dynamics, Part I: Open-loop systems, *Computer Methods in Applied Mechanics and Engineering*, **71**, 293–314, 1988.

[13] S. C. Wu, and E.J. Haug, Geometric non-linear substructuring for dynamics of flexible mechanical systems. *International Journal for Numerical Methods in Engineering*, **26**, 2211–2226, 1988.

ISBN 978-2-8052-0116-5